Computation of the response function in Chirp-Pulse Microwave Computerized Tomography

M Bertero§, F Conte†, M Miyakawa‡and M Piana†

§ INFM and DISI, Universita' di Genova, Via Dodecaneso 35, I-16146 Genova, Italy
† INFM and DIFI, Universita' di Genova, Via Dodecaneso 33, I-16146 Genova, Italy
‡ Department of Biocybernetics, Faculty of Engineering, Niigata University, 8050 Ikarashi2, Niigata 950-2181, Japan

Abstract. Chirp-Pulse Microwave Computerized Tomography (CP-MCT) is a technique designed to image temperature variations inside a body. In the prototype developed at Niigata University images are obtained by means of the basic algorithm of tomography, namely the filtered backprojection. The purpose of this paper is to develop an improved linear model for data reduction. We introduce a method, based on scattering theory, for computing the projections of a small phantom and we use these projections for defining the response function of the system. Our results also indicate that CP-MCT data are related to the variations of the attenuation constant inside a body. We conclude that, if these variations are sufficiently smooth, then CP-MCT projections can depend linearly on the distribution of the attenuation constant through the response function of the system.

1. Introduction

Chirp-Pulse Microwave Computerized Tomography (CP-MCT) [1, 2] is a technique which has been designed for providing maps (images) of temperature variations, via temperature dependence of the attenuation and/or phase constant of the microwaves. The scanning geometry of the prototype developed at Niigata University is precisely that of the first-generation X-ray tomographic scanners: two microwave antennas, one transmitting (the source S) and one receiving (the receiver R), are moved along two parallel lines which define the plane to be imaged; then the system is rotated by a certain angle and the scanning operation is repeated; the system is rotated again and so on up to cover the angle π. In the prototype fifty equispaced directions are used.

For each position of the source-receiver (S-R) pair Microwave Time Delay Spectroscopy (MTDS) [3] is used to extract from the received signal the contribution of the wave propagating along the straight path joining the two antennas. The technique is the following: a chirp signal is fed both to the transmitting antenna and to a mixer where

it is multiplied by the received signal; the output of the mixer is analysed by means of a band-pass filter to extract the amplitude of the beat frequency associated with the straight path joining the two antennas. For a fixed rotation angle the logarithms of these amplitudes, corresponding to the various positions of the S-R pair, provide a projection *in the sense of CP-MCT* of a physical quantity related to the spatial variations of the attenuation constant of the target. Then it is assumed that this projection can be approximated by the projection *in the Radon sense* of the same quantity. Finally the basic algorithm for Radon transform inversion, the *filtered back-projection* (FBP), is used to recover the map of the variations of the attenuation constant.

The advantage of this technique with respect to conventional microwave tomography is twofold [2]: the improvement of resolution due to the pulse compression allowed by the use of a chirp signal and the use of a fast linear algorithm for data inversion. Indeed, even if the problem is basically nonlinear, the very promising results obtained by means of FBP indicate that the process can be conveniently represented by a suitable linear model.

In a previous paper [4] we proposed to improve data inversion by a two-steps method: deconvolution of the projections by means of the response function of the system (supposed to be space-invariant) and subsequent use of FBP. The response function was obtained by a suitable processing of the projection of a cylinder immersed in a homogeneous absorbing medium (characterized by a different attenuation constant) and placed at the centre of the observation region.

The purpose of this paper is to provide a further improvement of the model given in [4]. We first give a very simple method for computing the projections of a phantom with a small spatial extent and we use this result for investigating the response function of the system. It turns out that this function is, in general, space-variant so that we can propose a quite natural generalization of the previous model.

The starting point is a 2D representation of the process of data acquisition in CP-MCT. The analysis is performed in frequency domain and the basic step is the solution of the scattering integral equation (the so-called *Lippmann-Schwinger equation*) [6] for all time frequencies corresponding to a chirp signal. If the spatial extent of the scatterer is small with respect to the wavelength of the emitted radiation, by means of a suitable approximation, it is possible to obtain a simple expression of the solution, which can be further simplified by means of the asymptotic expression of the Hankel functions for large values of the argument. As a result we obtain a procedure for computing the response function, much more efficient than those based on the solution of Maxwell equations in time domain, such as FD-TD [5].

In Section 2 we consider the propagation of the electromagnetic wave emitted by a line source supplied with a chirp signal in the case of a homogeneous absorbing medium (the bolus). In Section 3 we extend the analysis to the case of phantom immersed in the

bolus while in Section 4 we give the approximate solution of the Lippmann-Schwinger equation in the case of a phantom with a small spatial extent. The simplified expression of this solution, as provided by Born approximation, is also given as well as a computable expression of the correction term.

In Section 5 we outline the method for computing the projections of a pixel modeled as a small cylindrical phantom immersed in a bolus and we stress the symmetry properties of these projections. Numerical experiments are described in Section 6, in the particular case where the small phantom is located at the centre of the observation region, with a diameter of few millimiters. In one case we compare our result with that obtained by means of the FD-TD method. We find that the agreement is quite good. Then, due to the simplicity of our method, we can compute the projection of the phantom for several values of the contrast between the attenuation constant of the phantom and that of the bolus. We find that the integral of this projection is proportional to the contrast with a good approximation (2%) while the shape of the projection slightly depends on the contrast. In Section 7 these results are used for defining the response function of the system and for formulating our linear model in terms of this function. We show that, with some additional assumptions, we reobtain the linear model considered in [4].

The model given in Section 7 provides an improvement of the linear model used for data reduction in CP-MCT, namely the Radon transform. However the use of the improved model for the restoration of CP-MCT images requires the inversion of a large, non-sparse and ill-conditioned matrix. As concerns computational complexity similar problems must be solved, for instance, in PET or SPECT imaging. As it is well known, efficient iterative regularization methods can be used in these cases [7] and therefore we are planning to apply them to CP-MCT. Some conclusions are given in Section 8.

2. Wave propagation in a homogeneous absorbing medium

We consider first the propagation of an electromagnetic wave in a homogeneous isotropic absorbing medium (for instance a saline solution), which will be called the *bolus*, and we represent the electromagnetic fields $\mathcal{E}(x,t)$, $\mathcal{H}(x,t)$ in terms of their time Fourier transforms $\hat{\mathcal{E}}(x,\omega)$,$\hat{\mathcal{H}}(x,\omega)$, where ω is the time frequency

$$\mathcal{E}(x,t) = \frac{1}{2\pi}\int_{-\infty}^{+\infty} \hat{\mathcal{E}}(x,\omega)e^{-i\omega t}d\omega \quad , \tag{2.1}$$

$$\mathcal{H}(x,t) = \frac{1}{2\pi}\int_{-\infty}^{+\infty} \hat{\mathcal{H}}(x,\omega)e^{-i\omega t}d\omega \quad . \tag{2.2}$$

If we denote by ϵ_b and σ_b the relative dielectric constant and the electric conductivity of the bolus (which in general depend on the time frequency, $\epsilon_b = \epsilon_b(\omega)$, $\sigma_b = \sigma_b(\omega)$, and

in such a case satisfy the simmetry relations $\epsilon_b(\omega) = \epsilon_b(-\omega)$, $\sigma_b(\omega) = \sigma_b(-\omega)$) and if we also assume that the relative magnetic permittivity is equal to 1, then $\hat{\mathcal{E}}(x,\omega)$,$\hat{\mathcal{H}}(x,\omega)$ are solutions of the Maxwell equations in a source-less region

$$\nabla \wedge \hat{\mathcal{E}}(\cdot,\omega) - i\mu_0\omega\hat{\mathcal{H}}(\cdot,\omega) = 0 \tag{2.3}$$

$$\nabla \wedge \hat{\mathcal{H}}(\cdot,\omega) + i\epsilon_0\omega\left(\epsilon_b + i\frac{\sigma_b}{\omega\epsilon_0}\right)\hat{\mathcal{E}}(\cdot,\omega) = 0 \quad . \tag{2.4}$$

Next we introduce the following notations: we denote by k_0 the free-space wave number associated with the time frequency ω

$$k_0^2 = \epsilon_0\mu_o\omega^2 = (\omega/c)^2 \tag{2.5}$$

and by $k_b = k_b(\omega)$ the complex wave number in the bolus

$$k_b^2 = k_0^2\left(\epsilon_b + i\frac{\sigma_b}{\epsilon_0\omega}\right) \quad . \tag{2.6}$$

Then, from equations (2.3)-(2.4) it is possible to obtain the vector Helmholtz equation for $\hat{\mathcal{E}}(x,\omega)$

$$\triangle\hat{\mathcal{E}}(\cdot,\omega) + k_b^2\hat{\mathcal{E}}(\cdot,\omega) = 0 \quad . \tag{2.7}$$

We assume that the system is invariant with respect to translations in the direction of the x_3-axis and we restrict our analysis to the case of TM polarized electromagnetic fields (i.e. the electric field oscillates along the x_3 axis), so that $\hat{\mathcal{E}}_1 = \hat{\mathcal{E}}_2 = 0$ and the problem becomes two-dimensional. We denote by $\hat{u}$ the component $\hat{\mathcal{E}}_3$ of $\hat{\mathcal{E}}$, which is a function of x_1, x_2 and ω: $\hat{u} = \hat{u}(x_1, x_2, \omega)$. In the following we also denote by x the 2D vector with components x_1, x_2.

We introduce the particular solution corresponding to a line source located in the origin of the coordinates system and emitting a cylindrical wave with fixed frequency ω. It is given by

$$\Phi(|x|,\omega) = \frac{i}{4}H_0^{(1)}(k_b|x|) \tag{2.8}$$

with $Imk_b \geq 0$. If we put

$$k_b = \beta_b + i\alpha_b \tag{2.9}$$

where α_b and β_b are respectively the attenuation constant and the phase constant of the bolus, then we have

$$\alpha_b = |\omega|\sqrt{\frac{\epsilon_0\mu_0\epsilon_b}{2}\left[\sqrt{1+\left(\frac{\sigma_b}{\omega\epsilon_0\epsilon_b}\right)^2} - 1\right]} \quad , \tag{2.10}$$

$$\beta_b = \omega \sqrt{\frac{\epsilon_0 \mu_0 \epsilon_b}{2} \left[\sqrt{1 + \left(\frac{\sigma_b}{\omega \epsilon_0 \epsilon_b} \right)^2} + 1 \right]} \quad . \tag{2.11}$$

Therefore, if the emitting antenna is represented as a line source supplied with a chirp signal and x_S is the position of the source, then the Fourier transform of the field emitted by the antenna is given by

$$\hat{u}_b(x, x_S; \omega) = \hat{c}(\omega) \Phi(|x - x_S|, \omega) \tag{2.12}$$

where $\hat{c}(\omega)$ is the Fourier transform of a chirp signal $c(t)$ given by

$$c(t) = A\chi(t) \sin(\omega_1 t + \frac{1}{2} K t^2). \tag{2.13}$$

Here $\chi(t)$ is the characteristic function of the interval $(0, T_S)$ (T_S =sweep time) and K is the constant

$$K = \frac{\omega_2 - \omega_1}{T_S}. \tag{2.14}$$

The signal detected by a receiver at the point x_R is given by the inverse Fourier transform of $\hat{u}_b(x_R, x_S; \omega)$

$$u_b(x_R, x_S; t) = \frac{1}{2\pi} \int_{-\infty}^{+\infty} \hat{c}(\omega) \Phi(d, \omega) e^{-it\omega} d\omega \tag{2.15}$$

where d is the distance between the source and the receiver.

According to MTDS $u_b(x_R, x_S; t)$ is supplied to a mixer where it is multiplied by the chirp signal itself so that the output of the mixer is

$$s_{M,b}(x_R, x_S; t) = c(t) u_b(x_R, x_S; t) \quad . \tag{2.16}$$

The typical behaviour of the power spectrum of this signal is shown in Figure 1. It has a peak in correspondence of the beat frequency ω_B associated with the component of the detected signal propagating along the straight path joining the two antennas. Such a beat frequency is given by $\omega_B = KT$, where K is defined in equation (2.14) and T is the time delay between the reference signal $c(t)$ and the signal propagating along the straight line joining the two antennas, i.e. $T = d/c_b$, with c_b denoting the phase velocity in the bolus. The logarithm of the height of the peak is the value of the CP-MCT projection corresponding to the given position of the two antennas.

In the case of a homogeneous and isotropic medium, as that we are considering in this Section, the values of the projections depend only on the distance between the two antennas and therefore are constant if this distance remains constant during the scanning procedure. In order to understand what physical quantity is related to this constant value we can approximate $u_b(x_R, x_S; t)$ by means of the well-known asymptotic formula of the Hankel function for large values of the argument [8]

$$H_0^{(1)}(z) \simeq \sqrt{\frac{2}{\pi}} e^{-i\frac{\pi}{4}} \frac{e^{iz}}{\sqrt{z}} \tag{2.17}$$

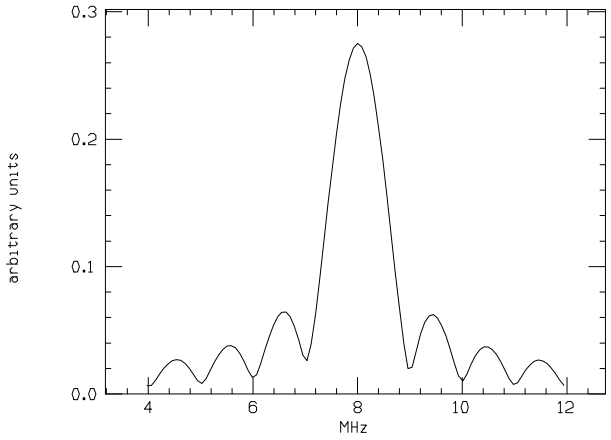

Figure 1. Power spectrum of the signal at the exit of the mixer (arbitrary units) as a function of frequency (MHz) in the case of a homogeneous and absorbing medium. The frequency of the maximum corresponds to the beat frequency $\omega_B = KT$.

and the result is

$$u_b(x_R, x_S; t) \simeq \frac{i}{4(2\pi^3)1/2} e^{-i\frac{\pi}{4}} \int_{-\infty}^{+\infty} \hat{c}(\omega) \frac{e^{idk_b}}{\sqrt{dk_b}} e^{-it\omega} d\omega \quad . \tag{2.18}$$

A further simplification can be obtained if we observe that, at first order in $(\sigma_b/\omega\epsilon_0\epsilon_b)^2$, α_b and β_b can be approximated as follows

$$\alpha_b \simeq \frac{1}{2}\sqrt{\frac{\sigma_b^2 \mu_0 \epsilon_b}{\epsilon_0}} \tag{2.19}$$

$$\beta_b \simeq \frac{\omega}{c_b} \quad , \tag{2.20}$$

with $c_b = (\epsilon_0 \mu_0 \epsilon_b)^{-1/2}$ the phase velocity in the bolus. If we use these approximations in equation (2.18) and exploit the fact that α_b is now independent of ω, we obtain

$$u_b(x_R, x_S; t) \simeq \frac{i}{4(2\pi^3)^{1/2}} e^{-i\pi/4} e^{-d\alpha_b} \int_{-\infty}^{+\infty} \frac{\hat{c}(\omega)}{\sqrt{d(\beta_b + i\alpha_b)}} e^{i(\frac{d}{c_b} - t)\omega} d\omega. \tag{2.21}$$

This equation, inserted in equation (2.16), shows that the logarithm of the signal at the exit of the mixer depends linearly on the quantity $\alpha_b d$, namely the integral of the attenuation constant along the straight path joining the two antennas. Such a simple interpretation, however, is no longer true in the general case.

3. The case of a phantom immersed in a bolus

We consider now the case of a non-homogeneous absorbing medium, the phantom, immersed in a homogeneous one, the bolus. We denote by Ω the bounded domain occupied by the phantom. Inside Ω the electrical parameters are functions of x and will be denoted by $\epsilon(x)$ and $\sigma(x)$, $\epsilon(x)$ being the relative electrical permittivity and $\sigma(x)$ the electrical conductivity. We also assume that the relative magnetic permittivity is equal to 1. Outside Ω the electrical parameters are again ϵ_b and σ_b. Therefore the Fourier Transforms of the electromagnetic fields satisfy in Ω the following Maxwell equations

$$\nabla \wedge \hat{\mathcal{E}} - i\omega\mu_0\hat{\mathcal{H}} = 0 \quad , \quad x \in \Omega \tag{3.1}$$

$$\nabla \wedge \hat{\mathcal{H}} + i\omega\epsilon_0\epsilon(x)\hat{\mathcal{E}} = \sigma(x)\hat{\mathcal{E}} \quad , \quad x \in \Omega \tag{3.2}$$

while, outside Ω, they satisfy the Maxwell equations (2.3)-(2.4).

If we consider again a TM polarized incident field and we assume traslation invariance of the phantom in the x_3-direction, the electric field can be written as $\hat{\mathcal{E}} = (0, 0, \hat{u})$ and the scalar field $\hat{u}$ inside Ω is a solution of the equation

$$\triangle\hat{u} + k^2(x)\hat{u} = 0 \tag{3.3}$$

with $k^2(x)$ given by

$$k^2(x) = k_0^2\left(\epsilon(x) + i\frac{\sigma(x)}{\epsilon_0\omega}\right) \tag{3.4}$$

while outside Ω is a solution of the equation

$$\triangle\hat{u} + k_b^2\hat{u} = 0. \tag{3.5}$$

Moreover, if we introduce the quantity $m(x)$ defined by

$$m(x) = \epsilon_b - \epsilon(x) + i\frac{\sigma_b - \sigma(x)}{\epsilon_0\omega} \quad , \tag{3.6}$$

so that we have

$$k^2(x) = k_b^2 - k_0^2 m(x) \quad , \tag{3.7}$$

then equation (3.3) becomes

$$\triangle\hat{u} + k_b^2\hat{u} = k_0^2 m(x)\hat{u} \quad . \tag{3.8}$$

We consider now a solution of the equations (3.5) and (3.8) which corresponds to a line source located in a point x_S, outside Ω, and supplied with a chirp signal. In addition it behaves at infinity as an outgoing cylindrical wave. Such a solution, which will be denoted by $\hat{u}(x, x_S; \omega)$, is a perturbation of the solution $\hat{u}_b(x, x_S; \omega)$ given in equation (2.12) and therefore can be represented in the form

$$\hat{u}(x, x_S; \omega) = \hat{c}(\omega)\Phi(|x - x_S|, \omega) + \hat{u}^{sc}(x, x_S; \omega) \tag{3.9}$$

where $\hat{u}^{sc}$ is the scattered field satisfying the Sommerfeld radiation condition

$$\lim_{r\to\infty}\sqrt{r}(\frac{\partial\hat{u}^{sc}}{\partial r}-ik_b\hat{u}^{sc})=0 \quad . \tag{3.10}$$

As it is well-known the solution of this problem can be reduced to the solution of the Lippmann-Schwinger (L-S) integral equation

$$\begin{aligned}\hat{u}(x,x_S;\omega)&=\hat{c}(\omega)\Phi(|x-x_S|,\omega)-\\&-k_0^2\int_\Omega\Phi(|x-y|,\omega)m(y)\hat{u}(y,x_S;\omega)dy\end{aligned} \tag{3.11}$$

where we use the fact that $\Phi(|x-y|,\omega)$, as defined in equation (2.8), is the 2D Green function associated with Sommerfeld radiation condition. It is also well-known that the L-S equation has a unique solution for any ω under very broad conditions on $m(x)$ (for our purposes it is sufficient to assume that $m(x)$ is bounded) [6]. Therefore equation (3.11) can be uniquely solved, in principle, for any ω.

In the case of a weak scatterer, if we put $M=\sup_{x\in\Omega}|m(x)|$ and $A_{max}=\sup_{x\in\Omega}\int_\Omega|\Phi(|x-y|;\omega)|dy$ and if we assume that the inequality

$$k_0^2MA_{max}\ll 1 \tag{3.12}$$

holds true, then we can use Born approximation which is obtained by replacing in the integral of equation (3.11) $\hat{u}(y,x_S;\omega)$ with $\hat{c}(\omega)\Phi(|y-x_S|,\omega)$. The result is

$$\begin{aligned}\hat{u}(x,x_S;\omega)&=\hat{c}(\omega)\Phi(|x-x_S|,\omega)-\\&-k_0^2\hat{c}(\omega)\int_\Omega\Phi(|x-y|,\omega)m(y)\Phi(|y-x_S|,\omega)dy \quad .\end{aligned} \tag{3.13}$$

This approximation will be used for our computation of the response function of a pixel (modeled by a small cylinder with constant permittivity and conductivity), because we will show that in such a case the correction terms are sufficiently small.

By taking the inverse Fourier Transform of the frequency-dependent solution or of its Born approximation, we obtain the time-dependent solution $u(x,x_S;t)$ generated by the antenna supplied with the chirp signal. From equation (3.9) it follows that its value at the position x_R of the receiver can be written as follows

$$u(x_R,x_S;t)=u_b(x_R,x_S;t)+u^{sc}(x_R,x_S;t), \tag{3.14}$$

$u_b(x_R,x_S;t)$ being given by equation (2.15). This is the signal supplied to the mixer so that the output of the mixer is given by

$$\begin{aligned}s_M(x_R,x_S;t)&=c(t)u(x_R,x_S;t)=\\&=c(t)u_b(x_R,x_S;t)+c(t)u^{sc}(x_R,x_S;t).\end{aligned} \tag{3.15}$$

The first term, as discussed in Section 2, depends only on the distance between the two antennas and therefore it is a background term which remain constant if the two antennas are moved by keeping constant their distance.

Finally the peak value of the power spectrum of $s_M(x_R, x_S; t)$ must be extracted, for instance by means of a suitable filter. The logarithm of this quantity is the datum to be considered for image restoration.

4. Approximate solution in the case of a small phantom

According to the model developed in the previous Sections the basic step for computing the projections of a phantom in CP-MCT is to solve the L-S equation. In the general case this is a rather heavy computational task. Here we propose an approximate solution which applies to the case of a phantom with a small spatial extent. More precisely we consider the following particular situation:

- the domain Ω of the phantom is a circle with center x_P and radius a, small with respect to the wavelengths associated to the chirp signal;
- the phantom is characterized by constant electrical permittivity ϵ_P and constant electrical conductivity σ_P.

Under these hypotheses the integral of equation (3.11) can be approximated by neglecting the variation of $\hat{u}(y, x_S; \omega)$ over Ω; we obtain

$$\hat{u}(x, x_S; \omega) = \hat{c}(\omega)\Phi(|x - x_S|, \omega) - k_0^2 m_P \hat{u}(x_P, x_S; \omega) A(x, \omega) \tag{4.1}$$

where

$$A(x, \omega) = \int_{|y - x_P| \leq a} \Phi(|x - y|, \omega) dy \tag{4.2}$$

and

$$m_P = \epsilon_b - \epsilon_P + i \frac{\sigma_b - \sigma_P}{\epsilon_0 \omega} \quad . \tag{4.3}$$

With this approximation the solution of the L-S equation is reduced to the determination of $\hat{u}(x_P, x_S; \omega)$. If we write equation (4.1) in x_P and solve the corresponding linear equation for $\hat{u}(x_P, x_S; \omega)$

$$\hat{u}(x_P, x_S; \omega) = \hat{c}(\omega)\Phi(|x_P - x_S|, \omega) - k_0^2 m_P \hat{u}(x_P, x_S; \omega) A(x_P, \omega), \tag{4.4}$$

we obtain

$$\hat{u}(x_P, x_S; \omega) = \frac{\hat{c}(\omega)\Phi(|x_P - x_S|, \omega)}{1 + k_0^2 m_P A(x_P, \omega)} \quad . \tag{4.5}$$

Therefore the approximate solution of the L-S equation is given by

$$\hat{u}(x, x_S; \omega) = \hat{c}(\omega)\Phi(|x - x_S|, \omega) - k_0^2 m_P \frac{\hat{c}(\omega)\Phi(|x_P - x_S|, \omega)}{1 + k_0^2 m_P A(x_P, \omega)} A(x, \omega) \ . \tag{4.6}$$

When $x = x_R$, i.e. the field is computed at the receiver, equation (4.6) can be furtherly simplified by exploiting again the small size of the perturbation in the computation of $A(x_R, \omega)$, namely by taking

$$A(x_R, \omega) = \pi a^2 \Phi(|x_R - x_P|, \omega). \tag{4.7}$$

The result is

$$\hat{u}(x_R, x_S; \omega) = \hat{c}(\omega)\Phi(|x_R - x_S|, \omega) - \\ - \pi(ak_0)^2 m_P \frac{\hat{c}(\omega)\Phi(|x_P - x_S|, \omega)\Phi(|x_R - x_P|, \omega)}{1 + k_0^2 m_P A(x_P, \omega)}. \tag{4.8}$$

If condition (3.12) is satisfied, then Born approximation can be applied. In such a case, by means of the usual approximation for computing the integral extended to the small cylinder in equation (3.13), we obtain

$$\hat{u}(x_R, x_S; \omega) = \hat{c}(\omega)\Phi(|x_R - x_S|, \omega) - \\ - \pi(ak_0)^2 m_P \hat{c}(\omega)\Phi(|x_P - x_S|, \omega)\Phi(|x_R - x_P|, \omega). \tag{4.9}$$

By comparing equation (4.8) and equation (4.9) we conclude that the denominator in equation (4.8) represents the correction to the Born approximation.

Finally we remark that the values of the physical parameters we consider in our numerical experiments allow the use of the asymptotic expression of the Hankel function for large values of the argument, except in the case of the computation of $A(x_P, \omega)$. In particular, the Born approximation of $\hat{u}(x_R, x_S; \omega)$ can be expressed in the following simplified form

$$\hat{u}(x_R, x_S; \omega) \simeq \frac{i}{4}\hat{c}(\omega) \left\{ \sqrt{\frac{2}{\pi}} e^{-i\pi/4} \frac{e^{ik_b d}}{\sqrt{k_b d}} - \right. \\ \left. - \frac{1}{2} m_P (ak_0)^2 \frac{e^{ik_b(|x_p - x_S| + |x_p - x_R|)}}{k_b \sqrt{|x_p - x_S||x_p - x_R|}} \right\} \tag{4.10}$$

where equation (2.17) has been used.

5. Projections of a small phantom (pixel)

We first introduce the variables appropriate to describe the scanning geometry in the parallel-beam case, i.e. that used in the prototype at Niigata University. We refer to Figure 2 where S and R denote respectively the positions of source and receiver while P is that of the phantom/pixel. The origin O of the coordinate system is the intersection of the rotation axis of the scanner with the plane to be imaged.

If the two antennas move in the direction θ, then the projection of the phantom in the direction θ is a function of the variable s indicated in the figure where we also give the coordinates s_P, y_P of P with respect to the coordinate system defined by the unit vectors $\theta, \theta^{\perp}$.

Since we must deal with high-frequency signals, it is convenient to work directly with their Fourier transforms. In particular the Fourier transform of the signal at the output of the mixer can be computed as the convolution product of the Fourier transforms of

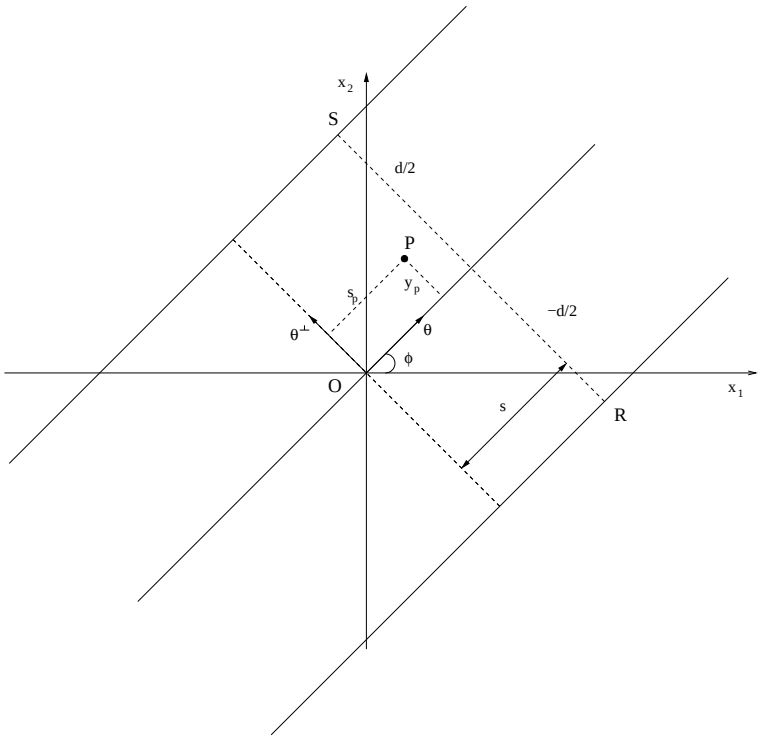

Figure 2. Scheme of the scanning geometry in CP-MCT; S and R denote respectively the position of the emitting and of the receiving antenna while P is the position of the small phantom (pixel). The variables θ and s are those used in the definition of the projections. We also give the coordinates s_P, y_P of P with respect to the coordinates system defined by $\theta, \theta^\perp$

the chirp and of the received signal. Therefore, for a given position of the S-R pair we have the following computational scheme:

- compute $\hat{u}(x_R, x_S; \omega)$ by means of equation (4.10);
- compute $\hat{s}(x_R, x_S; \omega)$ as the convolution product

$$\hat{s}_M(x_R, x_S; \omega) = \frac{1}{2\pi}(\hat{c} * \hat{u})(x_R, x_S; \omega); \tag{5.1}$$

- compute the maximum value of the modulus of $\hat{s}_M(x_R, x_S; \omega)$ (this is approximately the value of the modulus at the beat frequency $\omega_B = KT$);
- take the logarithm of the result;
- subtract the constant term due to the bolus.

For fixed θ the result of the last step, as a function of the position s of the S-R pair provides the CP-MCT *projection*, in the direction θ, of the phantom. As we see from

equation (4.10), this projection depends on the distances phantom-source and phantom-receiver, i.e. $r_{P,S} = |x_P - x_S|$ and $r_{P,R} = |x_P - x_R|$ respectively, and is symmetric with respect to the exchange of these quantities. These properties imply several relationships between different projections of different phantoms.

In order to exploit this point it is convenient to give the positions of source, receiver and phantom in terms of the coordinates defined by the unit vectors θ and $\theta^\perp$. We have (see Figure 2): $x_S = (s, d/2)$, $x_R = (s, -d/2)$, $x_P = (s_P, y_P)$, so that

$$r_{P,S} = \sqrt{(s - s_P)^2 + (y_P - \frac{1}{2}d)^2} \tag{5.2}$$

$$r_{P,R} = \sqrt{(s - s_P)^2 + (y_P + \frac{1}{2}d)^2}. \tag{5.3}$$

We find that, for all phantoms with positions corresponding to a given value of y_P, the projections are obtained by translating that of the phantom with $s_P = 0$. In addition, for a given value of s_P, the phantoms corresponding to y_P and $-y_P$ have the same projections. It follows that the projections of all phantoms in all directions can be obtained from the projections in the direction $\theta = (1, 0)$ of the phantoms with $s_P = 0$ and $y_P \geq 0$. Therefore, if we denote by $P(s, y_P)$ these projections, then the projection in the direction θ of a phantom located in the point x_P is given by

$$P_\theta(s) = P(s - s_P, |y_P|) \quad , \tag{5.4}$$

where s_P, y_P are just the coordinates of the point x_P in the system defined by the pair of unit vectors θ,$\theta^\perp$.

6. Numerical experiments

We use the computational scheme outlined above for investigating the projections of a phantom/pixel as functions of the electrical parameters of the phantom.

As concerns the features of the scanning system we assume that the distance between the two antennas is about 30 cm (more precisely 282 mm, because this is the value used in the prototype at Niigata University) and that the transmitting antenna is supplied with a chirp signal with frequency range from 1 to 2 GHz and sweep time of 200 ms. As concerns the bolus and the phantom we assume that they are saline solutions with frequency-independent electrical parameters, more precisely with values of the relative dielectric constant around 70 and values of the electric conductivity in the range from 1 to 2 Sm^{-1}. The list of the values used in our simulations is given in Table 1 where we also give the values of the corresponding attenuation constants. As reported in the Table they refer to saline solutions with different concentrations at different temperatures and corresponding to time frequencies in the range from 1 to 2 GHz.

temperature 32^o C, concentration 0.44%			
frequency (GHz)	1.0	1.5	2.0
ϵ	74.8	74.5	74.4
σ	0.97	1.19	1.50
α	21.1	25.9	32.6
temperature 32^o C, concentration 0.69%			
frequency (GHz)	1.0	1.5	2.0
ϵ	74.1	73.9	73.6
σ	1.56	1.78	2.08
α	33.5	38.5	45.3
temperature 37^o C, concentration 0.44%			
frequency (GHz)	1.0	1.5	2.0
ϵ	73.0	72.8	72.6
σ	1.14	1.33	1.60
α	24.9	29.1	35.0
temperature 37^o C, concentration 0.69%			
frequency (GHz)	1.0	1.5	2.0
ϵ	72.3	72.2	71.9
σ	1.67	1.87	2.13
α	36.3	40.9	46.9

Table 1. Values of the electrical relative permittivity, conductivity (Sm^{-1}) and attenuation constant (m^{-1}) used in our numerical experiments. They correspond to saline solutions with two different concentrations, at two different temperatures (both indicated in the Table) and for three values of the time frequency.

Moreover, in order to simplify the interpretation and the discussion of the numerical results, we consider the most simple case, that of a phantom located at the centre of the observation region. In all our computations we assume a diameter of 2.5 mm, even if this value is irrelevant because our approximations apply to the case where the size of the pixel is negligible, independently of its shape. We give this value because it is that used in a computation based on the FD-TD method, whose result is compared with that provided by our method.

In the case of the central pixel, the rotational symmetry of the system implies that we have only one projection, which is the function $P(s, 0)$ defined in the previous Section.

It can be obtained by means of the following expression of $\hat{u}(x_R, x_S; \omega)$, derived from equation (4.10), where the dependence on s is explicit

$$\hat{u}(x_R, x_S; \omega) \simeq \frac{i}{4}\hat{c}(\omega)\left\{\sqrt{\frac{2}{\pi}}e^{-i\pi/4}\frac{e^{ik_b d}}{\sqrt{k_b d}} - (ak_0)^2\frac{m_p e^{ik_b\sqrt{d^2+4s^2}}}{k_b(d^2+4s^2)^{1/2}}\right\} . \quad (6.1)$$

The power spectrum of $s_M(x_R, x_S; t)$ is computed by means of equation (5.1) and the logarithm of its peak value, followed by subtraction of the background term, provides the projection $P(s, 0)$ of the phantom.

As mentioned above, in one case we have compared our result with that obtained by means of a code based on the FD-TD method [9, 10, 11]. In this example the bolus is characterized by relative electrical permittivity equal to 73.9 and electrical conductivity equal to 1.78 Sm^{-1} (hence the values at 1.5 GHz for a saline solution with 0.69% concentration and temperature 32^o C - see Table 1) while the phantom is characterized by relative electrical permittivity equal to 74.5 and electrical conductivity equal to 1.19 Sm^{-1} (saline solution with 44% concentration and temperature 32^o C). As follows from Table 1 the bolus is more absorbing than the phantom and the contrast in the attenuation constant is about 33%. The results are shown in Figure 3 where the solid line corresponds to the projection obtained by means of the FD-TD method while the dashed line to the one obtained by means of our approximate method. The differences between the two results are not significant and concern mainly the side-lobes of the projections. The comparison has been performed after subtraction of the background term and normalization of the two projections to unit area. In the Figure we also indicate the size of the pixel. Since this is also he size of the Radon projection, we see that the disagreement betwen Radon and CP-MCT projection is dramatic.

Since the result obtained by means of FD-TD is also based on several approximations, the fact that we obtain practically the same result with two completely different computational schemes indicates the reliability of the two methods. However the advantage of the method proposed in this paper is that it can be easily implemented and used for computing the projections of several phantoms with different values of the contrast in the attenuation constant. Indeed, as it is obvious, our method can be implemented on a PC and is very fast. Therefore we can perform extensive computations with the aim of showing that the projection of a central phantom can be given in terms of a suitable response function.

We used the values of Table 1 for performing two numerical experiments: in the first the bolus is a homogeneous medium with electrical parameters corresponding to the maximum value of the attenuation constant as given in Table 1 (46.9 m^{-1}): in the second the bolus is a homogeneous medium with electrical parameters corresponding to the minimum value of the attenuation constant (21.1 m^{-1}). In both cases the electrical parameters of the phantom can take all other values given in Table 1. Therefore, in

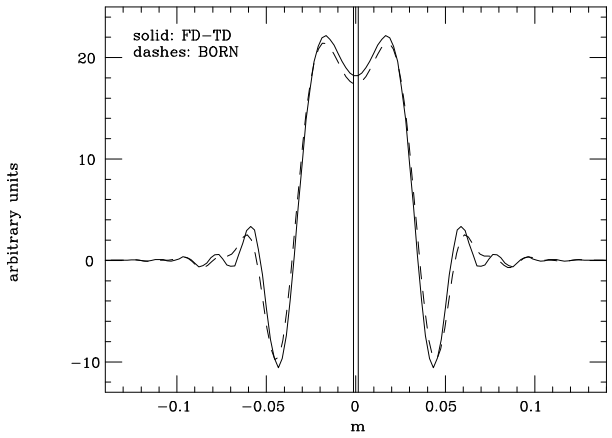

Figure 3. Projection of a centred circular phantom as given both by the FD-TD method (solid line) and by our approximate method (dashed line). In both cases the projections are normalized to unit area. The solid vertical lines indicate position and size of the phantom. The values of the physical parameters used in these computations are given in the text.

the first experiment the phantom is less absorbing than the bolus with a contrast in attenuation ranging from 3.5 to 57% while in the second the phantom is more absorbing than the bolus with a contrast ranging from 18 to 122%.

As concerns the validity of Born approximation, for all the situations considered in our experiments we have computed the quantity defined in equation (3.12) which provides an upper bound of the correction term in the denominator of equation (4.8). We have found that this quantity does not exceed 0.01 even in the case of the highest contrast and therefore the accuracy of Born approximation is of the order of 1%.

A first interesting result is the following one. For all computed projections, after background subtraction, we have evaluated the integral and we have found that, with a good approximation, it is proportional to the contrast in the attenuation constant (i.e., the difference between the attenuation constant of the bolus and that of the phantom). Indeed the ratio between the contrast and the integral of the projection of the pixel is extremely stable: in the case of the first experiment the average ratio is 2.46×10^5 with standard deviation 0.05×10^5 while in the case of the second experiment the average ratio is 2.25×10^5 with standard deviation 0.04×10^5.

Such a result suggests that the projection of a pixel can be described in terms of a response function if the shape of the projection is approximately independent of the constrast. The comparison of the projections can be easily performed if they

are normalized to the same integral (for instance unit integral). The results obtained from the two numerical experiments, after this normalization, are reported in Figure 4. In Figure 4 (a) we superimpose the projections of the phantoms considered in the first experiment while in Figure 4 (b) we superimpose the projections of the phantoms considered in the second experiment. In the framework of each one of the two experiments the differences are not very large and concern mainly the structure of the central lobe of the projections; in both cases the central minimum becomes deeper when the contrast increases. In addition it must be observed a difference in the side-lobes between the projections of Figure 4 (a) (less absorbing case) and those of Figure 4 (b) (more absorbing case). In any case the differences we have found are not dramatic.

In conclusion the results of our numerical experiments can be summarized as follows:

- the integral of the projection of a central pixel, modeled as a circular cylinder with a small radius, is approximately proportional to the contrast between the attenuation constant of the pixel and that of the bolus and therefore depends linearly on the value of the attenuation constant of the pixel;
- the shape of the projection is approximately independent of the attenuation constant of the pixel.

Some preliminary results indicate that these properties hold true also in the case of the projections of pixels located out of the centre of the region to be imaged.

7. The response function and the linear model

As pointed out in the Introduction, in the prototype developed at Niigata University the images are obtained by applying to the measured data the basic algorithm of tomography, namely the filtered backprojection. Such a procedure assumes that the data of CP-MCT can be described in terms of the Radon transform, i.e. are the line integrals of the quantity to be imaged. An equivalent description is obtained by considering each projection as a linear combination of the projections of the pixels located in the region to be imaged. The results of the previous Sections suggest a way for improving this model, namely to replace the Radon projections of a pixel with its CP-MCT projections as defined in Section 5.

The basic point is to define a sort of "average" response function which can be obtained, for instance, by computing the function $P(s, y), y > 0$, corresponding to a given contrast (let us say 30 or 40 %), both in the case of positive and in the case of negative contrast with respect to the bolus, and taking the arithmetic mean of the two results. This average projection can be normalized in such a way that its integral with respect to s is 1 for any value of y. This function, denoted by $R(s, y)$ has the property

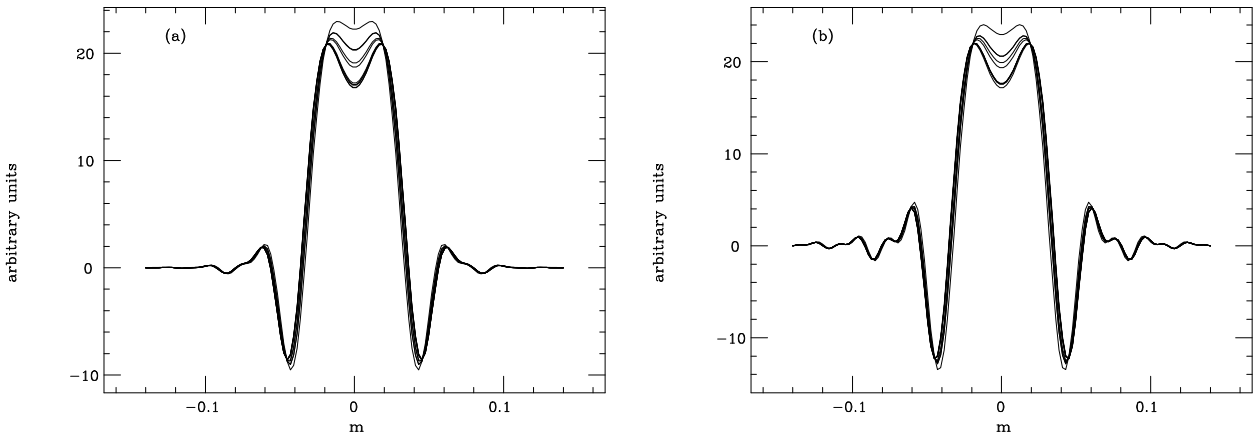

(a) (b)

Figure 4. Superposition of the projections of centred circular phantoms with different values of the attenuation constant. In (a) the phantoms are less absorbing while in (b) they are more absorbing than the bolus. In both cases the central minimum becomes deeper as the contrast with respect to the bolus increases. The values of the electrical parameters used in these numerical experiments are indicated in the text.

that the projections of an arbitrary pixel are approximately given by

$$P_\theta(s) \simeq c_P R(s - s_P, |y_P|) \tag{7.1}$$

where c_P is a constant proportional to the contrast between the attenuation constant of the pixel and that of the bolus. Therefore $R(s, y)$ can be called the *response function* of the system.

Now we consider again an extended phantom and we formulate the linear model whose validation for solving both the direct and the inverse problem of CP-MCT is in progress. We denote by $c(x')$ a function which is zero outside Ω, the domain of the extended phantom while in a point $x' \in \Omega$ takes a value proportional to the contrast between the attenuation constant of the phantom in x' and that of the bolus. Then we assume that the CP-MCT projection of the phantom in the drection θ is a linear superposition of the contributions of all its points, given in terms of the response function. For a fixed θ the result can be conveniently expressed in terms of the coordinates s', y' of x' with respect to $\theta, \theta^\perp$

$$g_\theta(s) = \int\int c(s', y') R(s - s', |y'|) ds' dy' \ . \tag{7.2}$$

We expect that this model applies at least to cases where the contrast variations inside the phantom are not too high so that the attenuation due to the reflection of the electromagnetic wave at the boundaries of the regions with the highest contrast can be neglected.

We would like to stress a few consequences of this model. First, if we assume that the response function is space-invariant, i.e. $R(s,y) \simeq R(s,0) = R(s)$, then we obtain

$$g_\theta(s) = \int R(s-s') \left(\int c(s',y')dy' \right) ds' \ . \tag{7.3}$$

It follows that, in such a case, *the CP-MCT projection is the convolution product of the Radon projection with the space-invariant response function R(s)*, i.e. we reobtain the model used in [4]. Our preliminary computations of the response function indicate that the condition of space-invariance is satisfied in a region around the origin of the scanning system but not everywhere. If the phantom is localized in the region of space-invariance then one can use the method of data reduction investigated in [4], namely deconvolution of the CP-MCT projections followed by FBP.

The second remark concerns the use of the more general model defined in equation (7.2) for data reduction. If the equation above is discretized by taking into account the discrete values of the scanning angles and of the positions of the S-R pair as well as by approximating the integral by a sum, then we get as a result that the vector of the data $\mathbf{g}$ is obtained by applying a very large matrix $\mathbf{R}$ to the vector $\mathbf{c}$ of the samples of the function to be imaged

$$\mathbf{g} = \mathbf{R}\mathbf{c} \quad . \tag{7.4}$$

Then the restoration problem consists in solving this linear system. However the matrix $\mathbf{R}$ is very large (it can have $10^4 \times 10^4$ elements since an oversampling of the data may be useful in practice - see [4]), is almost full and is ill-conditioned. The last property implies that regularization methods must be used for the approximate and stable solution of equation (7.4) [7] while the size of the matrix implies that it is necessary to use iterative methods with regularization properties such as the conjugate gradient. We are planning to use this and similar iterative methods for validating our model above in CP-MCT data reduction.

8. Concluding remarks

In this paper we have given a method which allows an easy and fast computation of the response function of CP-MCT, without using FD-TD or similar methods in time domain. Such a response function, as shown in the previous Section, has a typical behaviour: the central lobe has a structure similar to that of a pair of horns. Such a structure was not found in a previous paper [4]. The reason is due to the fact that in

that work the projection of a large cylinder was used to derive the response function by means of a deconvolution method. The limited information carried out by that kind of data, as already indicated in that paper, can explain the error in the evaluation of the response function. Anyway an analysis of data corresponding to cylinders with different diameters is in progress and is confirming the results obtained in this paper. It will be the subject of a subsequent publication. In conclusion we can say that our results are in a satisfactory agreement with the experimental data derived from the prototype at Niigata University.

Preliminary applications of the model described by equation (6.1) to the computation of the projections of very simple phantoms indicate that the results obtained in such a way are much more realistic than those provided by Radon transform. Therefore we expect an improvement also in the solution of the restoration problem. Work is in progress in this direction.

References

[1] Miyakawa M 1993 Tomographic measurements of temperature change in the phantoms of the human body by chirp radar-type microwave computed tomography *Med Biol Eng Comput* **31** S31-S36

[2] Miyakawa M 1996 Microwave imaging - 1: Microwave computed tomography in *Non-invasive Thermometry of Human Body* (M Miyakawa and J C Bolomey eds) CRC Press, Boca Ranton 105-126

[3] Jacobi J M and Larsen L E 1978 Microwave interrogation of dielectric targets. Part II: By microwave time delay spectroscopy *Med Phys* **5** 509-518

[4] Bertero M, Miyakawa M, Boccacci P, Conte F, Orikasa K and Furutani M 2000 Image restoration in chirp-pulse microwave CT (CP-MCT) IEEE *Trans Biomed Eng* **47** 600-609

[5] Taflove A 1998 *Advances in Computational Electrodynamics: The Finite-Difference Time-Domain Method* (Artech House, Cambridge)

[6] Colton D and Kress R 1992 *Inverse Acoustic and Electromagnetic Scattering Theory* (Springer, Berlin)

[7] Bertero M and Boccacci P 1998 *Introduction to Inverse Problems in Imaging* (IOP Publishing, Bristol)

[8] Abramowitz M and Stegun I 1972 *Handbook of Mathematical Functions* (Dover, New York)

[9] Furutani M, Miyakawa M, Hoshina S, Kanai Y and Ishii N 2000 *A numerical analysis of the tomographic imaging of the chirp radar-type micorwave computed tomography - Computation of the projection data based on a transfer function method* Technical Report of IEICE Japan AP98 **108** 13-18

[10] Orikasa K, Miyakawa M and Ishii N 2000 PSF-*based image restoration of* CP-MCT *by use of* FD-TD *method* Technical Report of IEICE Japan MBE99 **147** 13-18

[11] Kawada Y, Miyakawa M and Ishii N 1999 *Generation of tomographic images of* CP-MCT *based om* FD-TD *method* Technical Report of IEICE Japan MBE99 **82** 73-84